Available online at www.sciencedirect.com
ScienceDirect
Journal of Power Sources 161 (2006) 106–114
JOURNAL OF POWER SOURCES
www.elsevier.com/locate/jpowsour

SECM characterization of Pt–Ru–WC and Pt–Ru–Co ternary thin film combinatorial libraries as anode electrocatalysts for PEMFC

Guojin Lu *, James S. Cooper, Paul J. McGinn

Department of Chemical and Biomolecular Engineering, and Center for Molecularly Engineered Materials
University of Notre Dame, Notre Dame, IN 46556, United States

Received 28 March 2006; received in revised form 19 April 2006; accepted 20 April 2006
Available online 8 June 2006

Abstract

Rapid screening of electrocatalytic activity of ternary Pt–Ru–WC and Pt–Ru–Co thin film gradient material libraries towards hydrogen oxidation in the presence or absence of CO adsorption was performed by scanning electrochemical microscopy. It was observed that the addition of WC or Co to Pt or Pt-Ru catalysts can improve their hydrogen oxidation reaction activity and CO tolerance, making them suitable as potential electrocatalysts for polymer electrolyte membrane fuel cells. The stability of WC and Co in the acidic electrolyte were enhanced by alloying with Pt. SECM offers the capability for both qualitative and quantitative characterization of electrocatalytic activity of thin films of potential fuel cell electrode material candidates. However, promising electrode compositions identified by this technique need to be verified by traditional electrode preparation and characterization techniques.

Keywords: PEMFC; Electrocatalyst; Scanning electrochemical microscopy (SECM); Hydrogen oxidation; Combinatorial discovery; Tungsten carbide; Pt–Co alloys

1. Introduction

Although steady progress has been achieved in the development of PEM fuel cells, their large-scale production and commercialization is still challenged by several factors. Material costs remain high while performance remains below desired levels. Performance is mainly limited by the insufficient activity of the fuel cell electrodes. For the anode, the inevitable presence of carbon monoxide (CO) in the fuel, which remains in the reformed gas (trace, ppm level) or as byproducts and/or intermediates from direct oxidation of liquid fuels, can poison Pt-based catalyst materials [1,2]. CO can strongly adsorb on the surface of Pt and block its catalytically active area, thereby significantly decreasing its reactivity, causing the so-called "CO poisoning" problem. Due to this reason, for an excellent anode catalyst in PEM fuel cells, it has to show not only high catalytic activity towards hydrogen oxidation, but also enhanced activity in the presence of CO.

Pt–Ru alloys are typically considered as the preferred electrocatalysts for MOR (methanol oxidation reaction), but suffer from high cost [3]. Thus, it is desired to reduce the noble metal catalyst loading and/or replace the noble metals by less expensive alternatives while still maintaining the performance level. Ternary Pt-based catalysts have been investigated in which a third oxophilic component such as Sn, Ir, Rh, Os, Mo, W, WO_3, or Re is added to promote CO oxidation at lower potentials [4–7].

Tungsten carbide has been studied extensively for fuel cell catalyst applications, because of its unique chemical and physical properties [8–16]. It has been shown to have promising properties for catalyzing the hydrogen oxidation reaction (HOR), the methanol oxidation reaction (MOR), and even for the oxygen reduction reaction (ORR), and is considered to be a possible substitute for Pt. For example, surface studies of surface modified C/W(1 1 1), showed that significant catalytic activity towards methanol decomposition could be achieved [8]. The effect of carbon monoxide on the electroxidation of hydrogen by WC was systematically studied by Burstein et al. and it was seen that the presence of CO in H_2 gas stream only caused a small reduction of 2–6% in the activity towards HOR [11]. Lee et al. showed that Pt/W_2C microsphere catalysts provided much better utilization of Pt than Pt-Ru/C catalysts, and that Ru could be entirely

* Corresponding author. Tel.: +1 574 631 5692; fax: +1 574 631 8366.
E-mail address: glu1@nd.edu (G. Lu).

0378-7753/$ – see front matter © 2006 Elsevier B.V. All rights reserved.
doi:10.1016/j.jpowsour.2006.04.089

replaced [12]. It was also shown that adding W_2C can improve the catalytic activity of Pt–Ru in a H_2-stream containing CO [13]. In a recent communication, high electrocatalytic activity towards HOR and relatively good performance were observed in a real fuel cell environment for nanoparticle WC anode catalysts prepared by mechanical milling, which was attributed to the inherent W-C valence and also to the particles' nanostructure [15].

Pt–Co alloys have also been found to be good electrochemical catalysts for the oxygen reduction reaction, as well as for methanol oxidation in acid solution [17–19]. In a recent publication by Strasser et al., it was shown both by high-throughout experiments and theoretical calculations that a Pt–Ru–Co alloy with the composition of Pt:Ru:Co 1:1:3 was extremely active towards methanol oxidation (8 times higher than that of Pt–Ru) [1].

Combinatorial materials synthesis and high-throughput screening has been applied to systematically and rapidly identify candidate materials for a wide range of applications, including the discovery of high performance catalysts for PEM fuel cells [20–24]. In previous publications, we described a plasma sputtering system for the deposition of combinatorial catalyst libraries for PEM fuel cells, and the quantitative screening of their electrocatalytic activity (reactivity imaging) by scanning electrochemical microscopy (SECM) [25–27]. The SECM system used consists of a three-dimensional positioning system and operates under feedback mode, which involves the measurement of electrochemical currents of an ultramicroelectrode (UME) tip that is scanned across a substrate at a controlled separation distance in the vicinity of the substrate [28].

In the present study, we report on the preparation of ternary Pt–Ru–WC and Pt–Ru–Co "composition spread" thin film catalyst libraries by sputtering, and screening of their catalytic activity towards HOR by scanning electrochemical microscopy. To the best knowledge of the authors, this article represents the first report in the literature studying tungsten carbide thin films as fuel cell electrocatalysts by combinatorial techniques.

2. Experimental

2.1. Catalyst sample preparation

Thin film catalyst libraries were prepared by plasma sputtering onto a 2″ silicon wafer. Prior to deposition, a 1000 Å Si oxide film was thermally grown on the surface. A base layer of 2000 Å-thick TiN was deposited by reactive sputtering onto the wafer to act as a diffusion barrier and electrode contact. Binary or ternary continuous composition gradients were then sputtered by overlapping stripes of varying thickness of desired components through a simple masking approach, as described in more detail elsewhere [27]. Pt, Ru and WC or Co targets of 99.99% purity were used. Stripes were typically deposited in 20 Å layers, alternating between the library components, with a total of 8 layers of each component (∼160 Å total). Post-deposition vacuum annealing at 130 °C for 8 h and then at 520 °C for 4 h was used to promote interdiffusion between the layers.

2.2. Scanning electrochemical microscopy characterization

Catalyst libraries were characterized for their electrochemical reaction activity with a scanning electrochemical microscope (UniScan SECM 270). A homemade Au microelectrode with a 25 μm diameter and a glass to metal ratio (Rg) greater than 10:1 was used. The feedback mode of the SECM was employed to measure the electrocatalytic activity of thin film samples toward the hydrogen oxidation reaction (HOR).

The electrochemical cell is composed of four electrodes with the tip as one working electrode and the sample substrate (Si wafer) as the other. The substrate was positioned at the bottom of the cell horizontally with the deposited surface facing upwards. A saturated calomel electrode (SCE, 0.242 V versus SHE) and Pt foil were used as the reference electrode and counter electrodes, respectively. In the description that follows, all the potentials are referred to SCE if not otherwise stated. After the annealed wafer is placed in the cell, it is leveled so that the sample surface is parallel to the x–y plane traversed by the microelectrode tip. The leveling procedure is critical to avoid image fading due to changes in tip-substrate separation during SECM characterization. The solution of 0.01 M H_2SO_4/0.1 M Na_2SO_4 electrolyte is then introduced into the cell. Before conducting catalytic characterization experiments, the tip is cleaned by sweeping cyclic voltammetry (CV) between −1.2 and +1 V at a scan rate of 50 mV s^{-1} for 10 cycles with the tip located at a long distance (over 500 μm) from the substrate. After cleaning, the steady-state tip current ($I_{T,\infty}$) is approximately −400 nA at −1 V. Following the tip cleaning procedure, an approach curve is measured to determine the tip-substrate separation. Thereafter, the tip is set 10 μm above the substrate surface and a surface area of 3 mm × 3 mm is scanned at a scan size of 50 μm and scanning rate of 50 μm s^{-1}. During the scanning, the substrate potential is set at 0 V while the tip is typically held at a constant potential of −1 V (versus SCE), a potential at which the tip reaction is the diffusion-limited reduction of protons to generate hydrogen

$$2H^+ + 2e^- \rightarrow H_2. \quad (1)$$

At very small tip-substrate separation, the tip-generated hydrogen can diffuse to the surface of the substrate sample, where it can be oxidized, creating a proton, if the sample surface is electrochemically active. The protons (H^+) can then diffuse back to the tip surface, where they are reduced by the reverse reaction of (1), resulting in additional tip current. The rate of hydrogen electro-oxidation into protons (H^+) at the substrate determines their concentration near the tip, and hence the probe tip current (I_T). Accordingly, the difference in relative tip current with position reflects the activity difference of the local sites of the sample toward hydrogen oxidation.

To investigate the effect of CO poisoning, the cell was first purged with 99.9% CO through a gas dispersion tube with porous ceramic frit for 30 min., while the substrate potential was set at −0.24 V. Then the cell was purged with N_2 for 20 min to remove dissolved CO in the electrolyte, with the substrate potential set at −0.10 V. After gas purging, a normal area scan was conducted

on the same sample area with the experimental conditions the same as the above-mentioned.

3. Results and discussion

The masking technique used permits simultaneous deposition of several binary or ternary composition spread library "crosses" on the substrate. A map of the as-deposited samples on a Si wafer is illustrated in Fig. 1. Crosses on the Si wafer form continuous binary or ternary composition gradient libraries between two or three materials. To ensure that reproducible measurements are achieved, copies of the same library are deposited on the same wafer. The square pads on the periphery are used for X-ray diffraction characterization when desired. The composition gradient occurs where the stripes overlap, across an area of 2 mm^2. The area of interest can be expanded or contracted by varying the shadow mask size and offset distance. A schematic representation of a 2-layer composition spread binary library can be seen in Fig. 2 before (A) and after (B) diffusion. Fig. 2A shows how the stripe thickness varies through the cross section. Also shown in Fig. 2B are the approximate compositions at different locations in the joint area. Extensive characterization of the variation of line thickness and composition was performed by a combination of profilometry, energy dispersive spectroscopy, and Auger electron spectroscopy to establish the actual composition distribution.

Fig. 3 shows a schematic diagram of a single layer ternary cross. Three overlapping stripes will continuously cover all possible compositions across a ternary phase field. A representation of the compositions achieved after annealing of the center ternary region inside the box of Fig. 3A is shown in Fig. 3B. The region in the center of the six pronged cross where all three stripes overlap contains the ternary compositions. Fig. 3C is a representation of the compositions in Fig. 3B mapped onto a ternary phase diagram.

Fig. 4 shows the SECM area scan images of a Pt–Ru binary cross before (Fig. 4A) and after CO adsorption (Fig. 4B). The direction of the Pt and Ru stripes are denoted by the black arrows, with the outer lines defining the approximate line edges. Although Ru itself shows only minimal activity towards HOR (Fig. 4A), alloying Ru with Pt is seen to increase the HOR activity of Pt, as indicated by the higher currents in the binary overlap region. Comparing Fig. 4A and B shows that unalloyed Pt areas exhibit activity before CO and a loss of activity after CO adsorption, while Ru additions significantly enhance the CO tolerance of Pt (Fig. 4B), as expected. The highest current for the sample with CO adsorption is found in the overlap region of the Pt–Ru cross. For the test conditions used here, we can only conclude that the optimum Pt content for CO poisoning resistance is between 20 and 70 at.%.

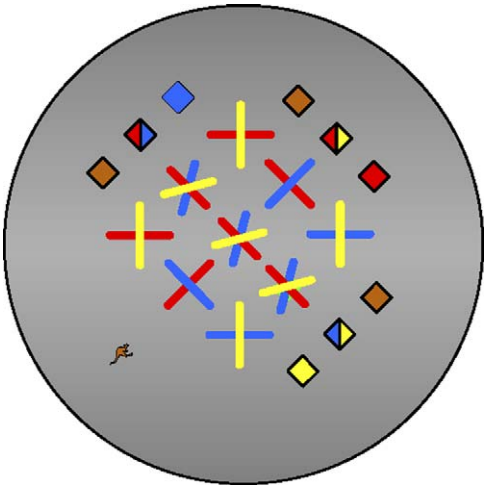

Fig. 1. Profile of the ternary gradient phase combinatorial library. Yellow stripes: Pt, Red stripes: Ru, Blue stripes: WC or Co or their substitutions.

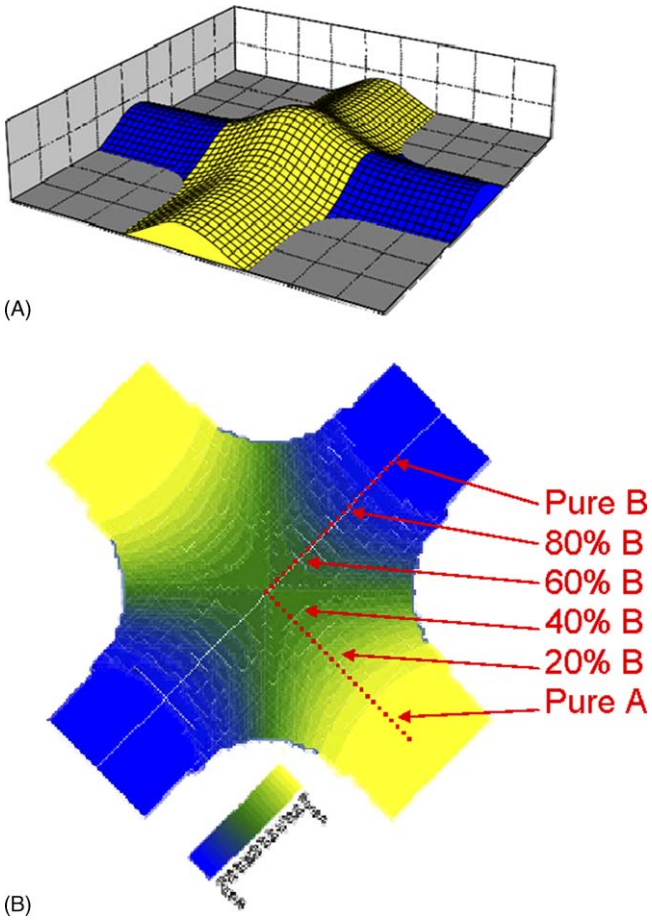

Fig. 2. (A) 3D representation of a binary cross A–B (e.g., A = Pt and B = Ru) continuous composition library before diffusion. (B) Diagram showing composition variation across the area of interest after diffusion.

The SECM area scan image of a ternary Pt–Ru–WC cross before CO adsorption is presented in Fig. 5A. Pt–Ru binary regions (triangles marked as 1) both show elevated activity relative to pure Pt. In addition, Pt–WC binary regions (triangles marked as 2) also show enhanced activity. The WC–Ru binary regions are relatively inactive. Within the Pt–Ru–WC ternary region, there are two regions showing HOR current lower than that of pure Pt itself. These regions lie within approximately 10% of $Pt_{60}Ru_{20}(WC)_{20}$.

The SECM area scan image of a ternary Pt–Ru–WC cross after CO adsorption is presented in Fig. 5B. Most Pt–Ru–WC regions exhibit superior CO tolerance compared to Pt, as indi-

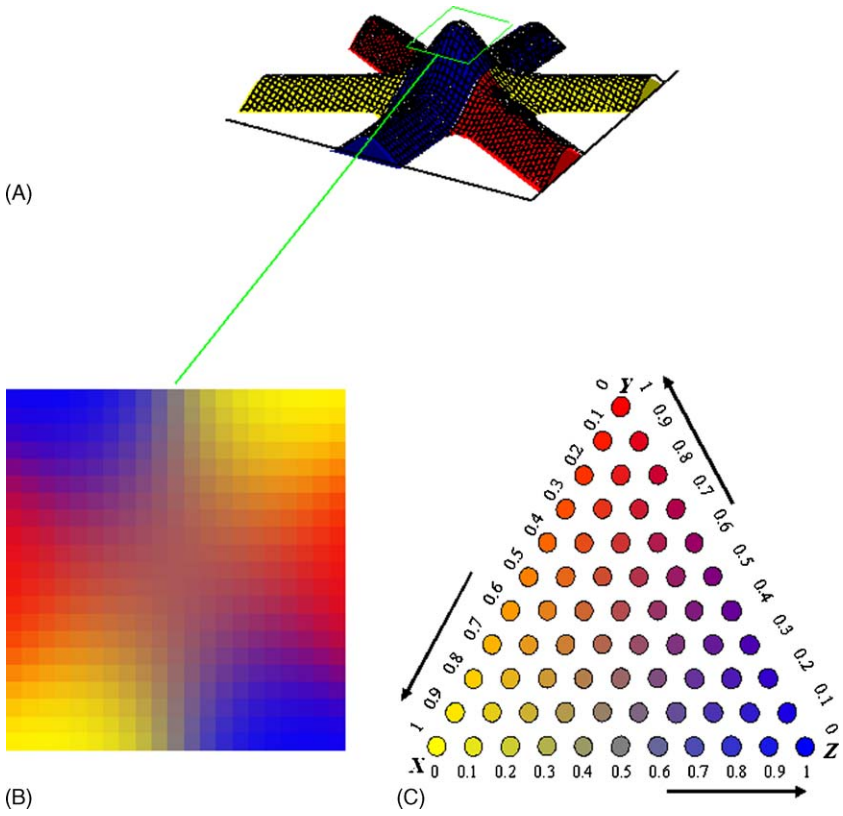

Fig. 3. (A) 3D representation of a ternary cross, now the overlapping stripes are at 60° instead of being perpendicular in the case of Fig. 2. (B) Composition profile for a ternary cross, where composition X, Y and Z are represented by different colors. The relationship between different colors and the corresponding compositions are illustrated in (C).

cated by the bright yellow central area and the two pink areas. The two yellow circular areas in Fig. 5A are now showing no HOR activity after CO poisoning, indicating almost no CO tolerance for these compositions. In the two pink areas (mostly in the Pt–Ru–WC joint area, some in the Pt–Co joint area), where the approximate composition is $Pt_{25\pm10}Ru_{5\pm5}(WC)_{70\pm5}$, the HOR activity is much higher than pure Pt, indicating high CO tolerance for these compositions. This result agrees partially with our multichannel microelectrode data for methanol oxidation on Pt–Ru–WC ternary systems, where the optimum composition at room temperature is $\sim Pt_{25}Ru_0(WC)_{75}$ [29].

Fig. 6 shows SECM area scan images of a Pt–WC binary cross before and after CO adsorption. As can be seen from Fig. 6A, when WC content is in the range of 30–85 at.%, the HOR activity of Pt is increased with the addition of WC. The same composition region also shows increased HOR current after CO adsorption compared to Pt, as indicated by the pink and orange current zones in Fig. 6B, signifying enhanced CO tolerance. The optimum composition lies where the WC content is between 65 and 80 at.%. This result again agrees with our multichannel microelectrode data for methanol oxidation on Pt–Ru–WC ternary systems [29].

The experimental data indicates that the addition of WC within a certain content range to Pt or Pt–Ru alloy catalysts can enhance both their HOR catalytic activity and CO tolerance. There are several possible mechanisms for the increased CO tolerance. It can be ascribed to a synergistic effect between Pt and WC, leading to high activity of tungsten carbide in the presence of Pt towards the dissociation of water and methanol [12]. It can also be attributed to the weaker bonding between tungsten carbide and CO, and therefore permitting relatively easy desorption of CO from WC [11,12]. Actually, on tungsten carbide, it was reported that the CO desorption temperature is at least 100 °C lower than on Pt [12]. The desorption temperature of CO from Pt/C/W(1 1 0) and Pt/C/W(1 1 1) is also significantly lower than from bulk Pt [3,9,30].

It is also noted that the maximum current values in Fig. 5B and 6B (after CO adsorption, 0.58 and 0.71 μA, respectively) are larger than the corresponding maximum values in Fig. 5A and 6A (before CO adsorption, 0.55and 0.62 μA, respectively). This interesting phenomenon can be explained by the fact that tungsten carbide can oxidize CO at the current substrate potential (0 V versus SCE), which can contribute extra hydrogen ions generated on the substrate and subsequently the extra hydrogen ions can diffuse to the tip and increase the tip current relative to that from the system without CO adsortion. This further verifies the high intrinsic activity of tungsten carbide towards CO oxidation and its strong CO tolerance. The CO oxidation can be written as the following:

$$\text{Pt-CO}_{\text{ads}} + \text{M-OH}_{\text{ads}} \rightarrow \text{Pt} + \text{M} + \text{CO}_2 + \text{H}^+ + \text{e}^- \quad (2)$$

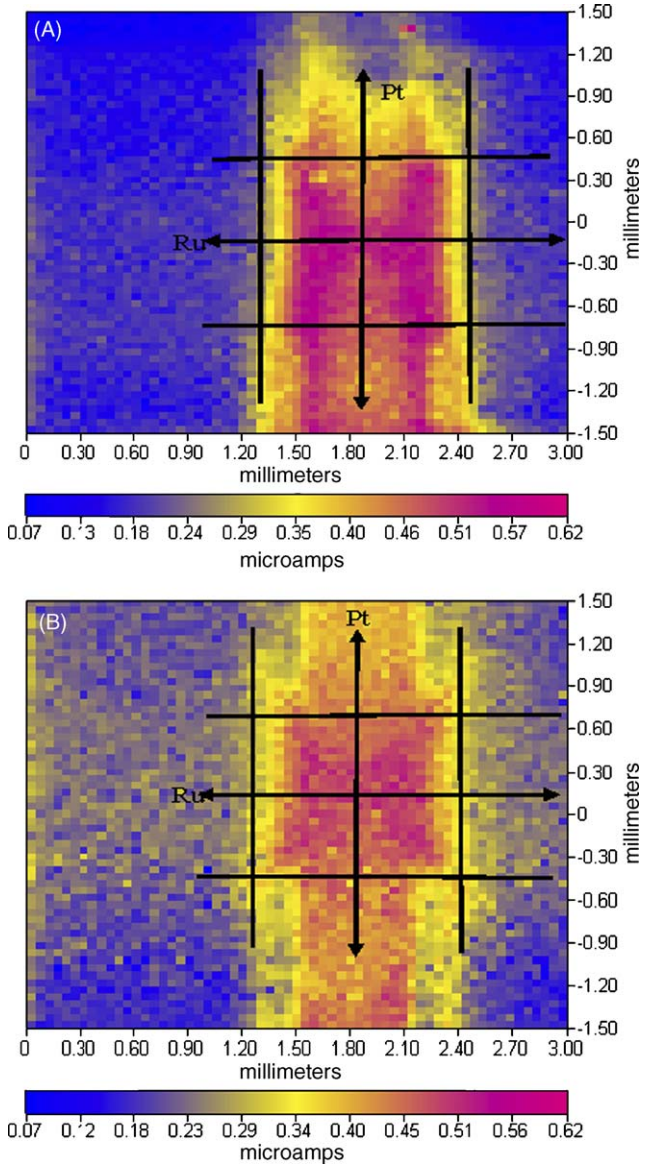

Fig. 4. SECM area scan images for a Pt-Ru thin film cross before (A) and after CO poisoning (B), (the tip was moved −300 μm in y direction after CO adsorption). $i_{T,\infty}$ is around 400 nA. $E_{tip} = -1\ V_{SCE}$, $E_{sub} = 0\ V_{SCE}$, separation between tip and substrate is 10 μm.

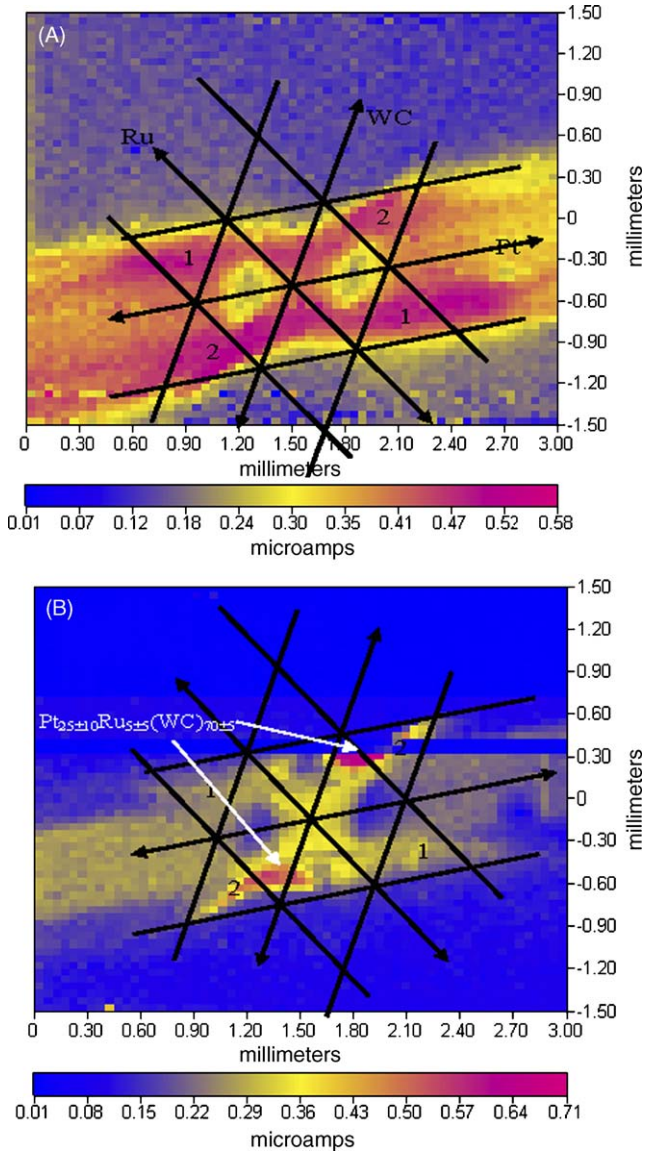

Fig. 5. SECM area scan images for a Pt–Ru–WC thin film cross before (A) and after CO poisoning (B, the tip was moved −500 μm in y direction after CO adsorption). $i_{T,\infty}$ is around 400 nA. $E_{tip} = -1\ V_{SCE}$, $E_{sub} = 0\ V_{SCE}$, separation between tip and substrate is 10 μm.

where M represents Pt, Ru or WC. Before this reaction, there is a preceding step of water dissociation reaction:

$$M + H_2O \rightarrow M\text{-}OH_{ads} + H^+ + e^- \quad (3)$$

The equilibrium potential of reaction (3) is about 0.45–0.55 V and 0.25 V (versus SHE, 0.2–0.3 and 0 V versus SCE) on Pt and Pt–Ru catalysts, respectively [31]. The exact potential of this reaction on WC is not known, but it should be much lower than that of Pt and we can assume it to be close to that of Pt–Ru. The equilibrium potential of reaction (2) is about 0.55 V (versus SCE) on Pt (onset potential 0.45 V), 0.25 V on Pt–Ru (onset potential 0.15 V), as determined by stripping CO cyclic voltammetry in 0.5 M H_2SO_4 [32,33]. By the same method, Fenton and co-workers found that tungsten carbide catalyst oxidizes CO at potentials as low as −0.06 V in 0.5 M H_2SO_4 and the onset CO oxidation potential is about −0.15 V [34]. Besides the CO oxidation peak at 0.5 V, another oxidation peak was identified at −0.06 V and attributed to CO oxidation on the WC surface. Considering the concentration of the sulfuric acid we used here is only 0.01 M, the above potential values should be about 0.1 V lower for the present study according to the Nernst's equation. It is apparent that both reaction (2) and (3) can occur on the surface of WC at the substrate potential (0 V) and both reactions can generate and supply the tip with some extra protons from the adsorbed CO. On the surface of Pt, neither reaction can occur. On the surface of Ru, only reaction (3) can happen and contribute part of the observed tip current increase. The current increase contributed from reactions (2) and (3) more than compensates

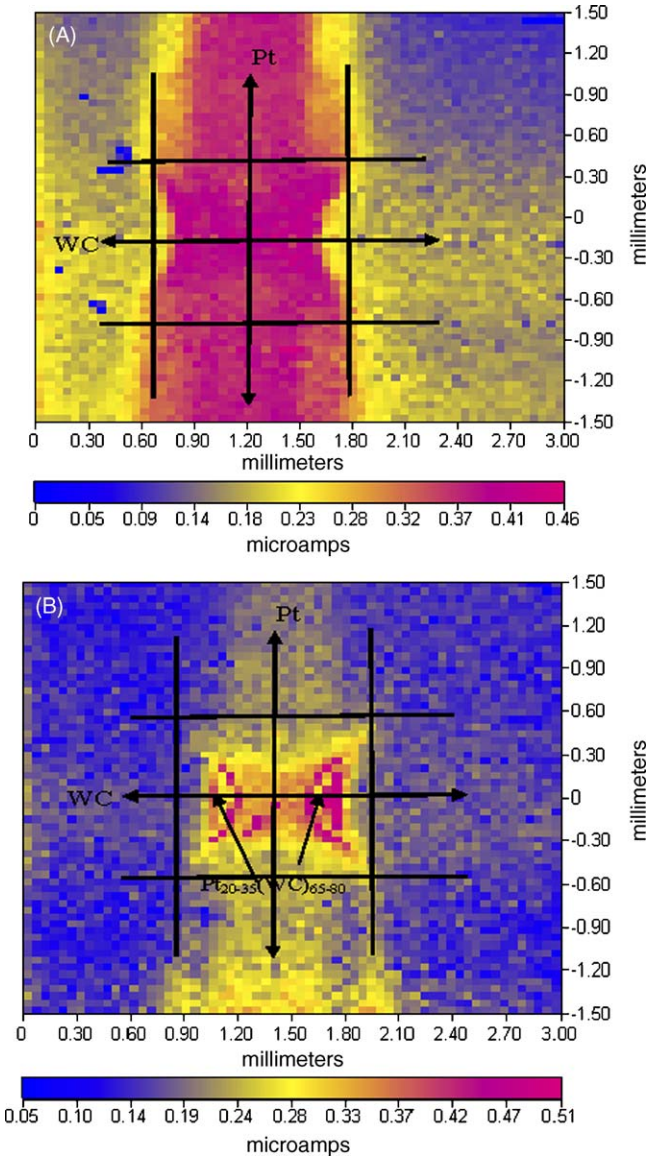

Fig. 6. SECM area scan images for a Pt-WC thin film cross before (A) and after CO poisoning (B, the tip was moved −300 μm in *x*-direction after CO adsorption). $i_{T,\infty}$ is around 400 nA. $E_{tip} = -1\ V_{SCE}$, $E_{sub} = 0\ V_{SCE}$, separation between tip and substrate is 10 μm.

for the current loss due to CO adsorption, so a larger current can be observed for some Pt–Ru–WC compositions even after CO adsorption.

Although WC incorporation into Pt or Pt–Ru can increase the HOR activity and CO tolerance, its stability is a concern. In the electrolyte solution of 0.01 M H_2SO_4 + 0.1 M Na_2SO_4, WC stripes disappeared (i.e., were dissolved) immediately after the immersion. Different conclusions can be found from the literature for the corrosion resistance of tungsten carbide. Some claim that pure WC has low corrosion resistance under acidic and oxidative conditions (e.g. H_2SO_4 with various pH values) [15,35]. Other reports, for example J.G. Chen et al., showed by electrochemical CV and XPS measurements that WC film is stable in 0.5 M H_2SO_4 at anodic potential below 0.6 V_{SHE} [36]. The reason for the discrepancy between our findings and their results is uncertain. One possible factor could be galvanic corrosion between WC and Pt or Ru since they are electrically connected by a conducting base material of TiN. However, this explanation can not be confirmed by the current experimental system and need to be verified with experiments on isolated WC samples. Another possibility is that there may be some sub-stoichiometric WC (e.g. WC_{1-x}), which may be less corrosion resistant than WC.

Although the pure WC stripe was not corrosion resistant in the current solution, HOR current increase and CO tolerance enhancement to Pt can still be observed, which is especially clear in the center area of Pt–WC binary library (Fig. 6). That means there is still some WC remaining in the center cross area and suggests that by alloying with Pt it is possible to increase its corrosion resistance and retain the excellent catalytic activity and CO tolerance of Pt–WC or Pt–Ru–WC alloys.

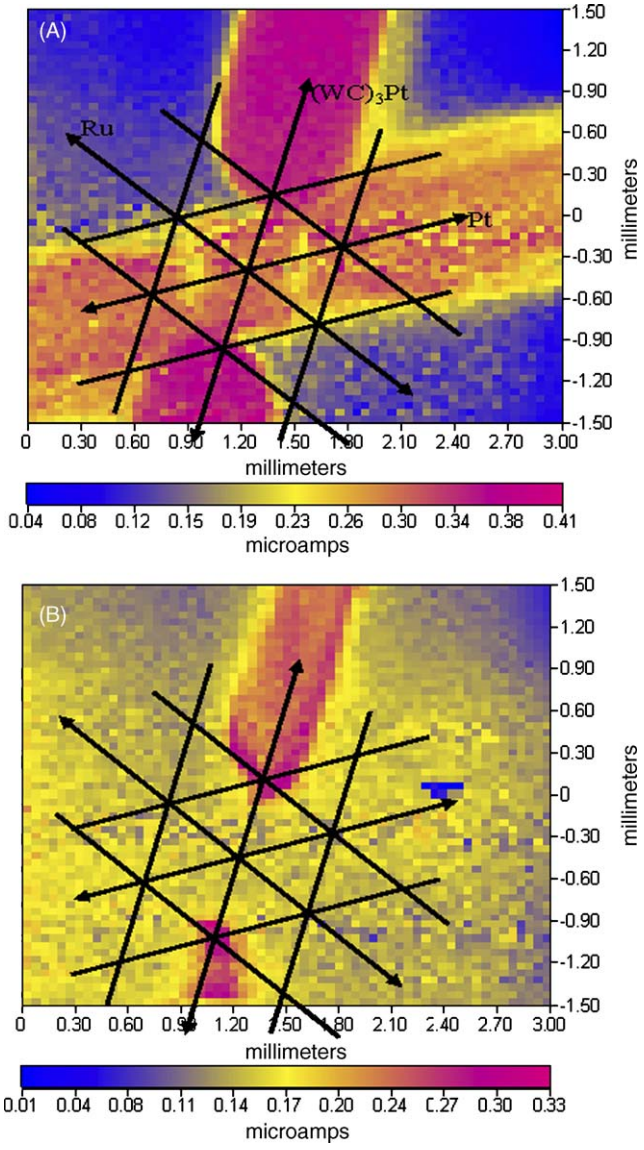

Fig. 7. SECM area scan images for a Pt-Ru-$(WC)_3$Pt thin film cross before (A) and after CO poisoning (B). $i_{T,\infty}$ is around 360 nA. $E_{tip} = -1\ V_{SCE}$, $E_{sub} = 0\ V_{SCE}$, separation between tip and substrate is 10 μm.

This idea was tested by substituting Pt for two of the 8 WC layers in the deposited stripe, giving an overall $Pt(WC)_3$ stoichiometry. By incorporating Pt, the corrosion resistance of WC is substantially improved. No apparent degradation occurred for the WC stripe even after immersion in the solution for several days.

The activity of $Pt(WC)_3$ towards HOR is also higher than that of WC or Pt alone, as shown in Fig. 7. The addition of Pt to the stripe of WC also improved the CO poisoning tolerance of Pt, as indicated by the fact that $Pt(WC)_3$ stripes retain most of their activity after CO poisoning.

As noted earlier, Pt-Co alloys have also been reported to show enhanced HOR activity. The SECM area scan image of a ternary Pt–Ru–Co cross before CO adsorption is presented in Fig. 8A. Again, as expected, Pt-Ru binary areas (including ternary areas with the incorporation of Co) exhibit enhanced HOR activity. Compositions of Pt–Ru–Co in the two pink areas (mostly in the Pt–Ru–Co joint area, some in the Pt–Co joint area), where the approximate composition is $Pt_{25\pm20}Ru_{15\pm15}Co_{60\pm15}$, show better HOR activity than binary Pt-Ru or Pt alone.

The SECM area scan image of the same ternary Pt–Ru–Co cross after CO adsorption is presented in Fig. 8B. All the compositions suffer CO poisoning and lose HOR activity to different extents, with the Pt stripe losing almost all of the activity. However, compositions of Pt–Ru–Co with the same compositions as the most active areas in Fig. 8A (pink area) show only limited activity loss (about 15%), indicating compositions in this area also have strong CO tolerance.

The above experimental data indicates that addition of Co to Pt or Pt–Ru alloy catalysts can enhance both their HOR catalytic activity and CO tolerance. There are several possible mechanisms that have been suggested for the improved CO tolerance [1]. Like Ru, Co is also an oxophilic metal and can facilitate

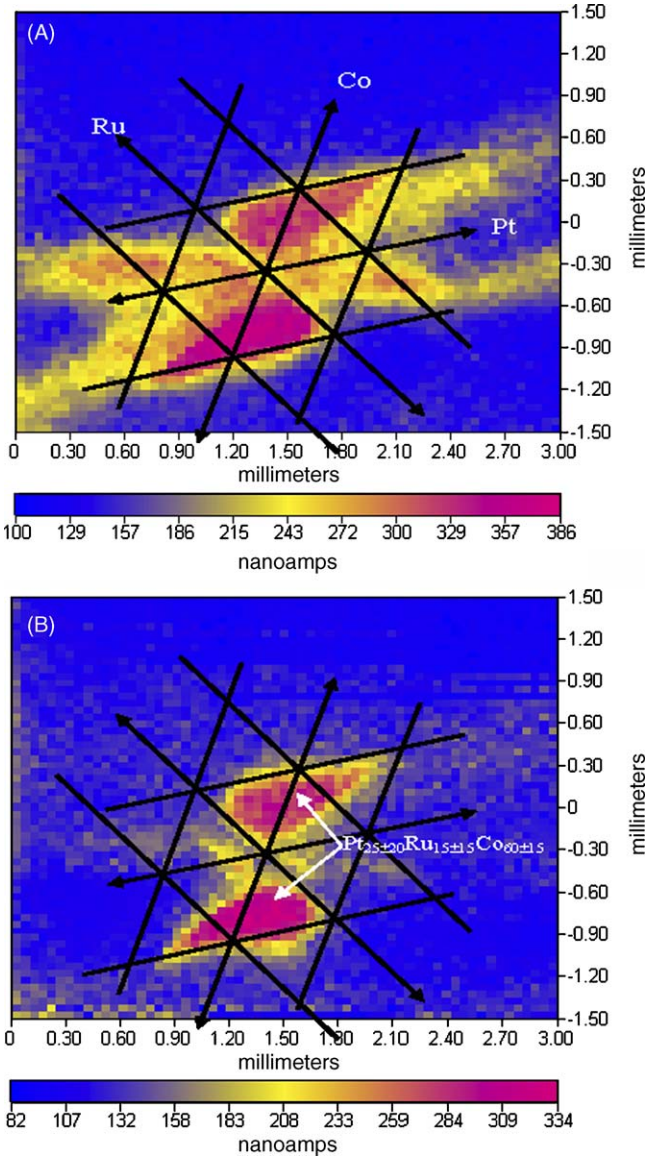

Fig. 8. SECM area scan images for a Pt–Ru–Co thin film cross before (A) and after CO poisoning (B). $i_{T,\infty}$ is around 350 nA. $E_{tip} = -1\ V_{SCE}$, $E_{sub} = 0\ V_{SCE}$, separation between tip and substrate is 10 μm.

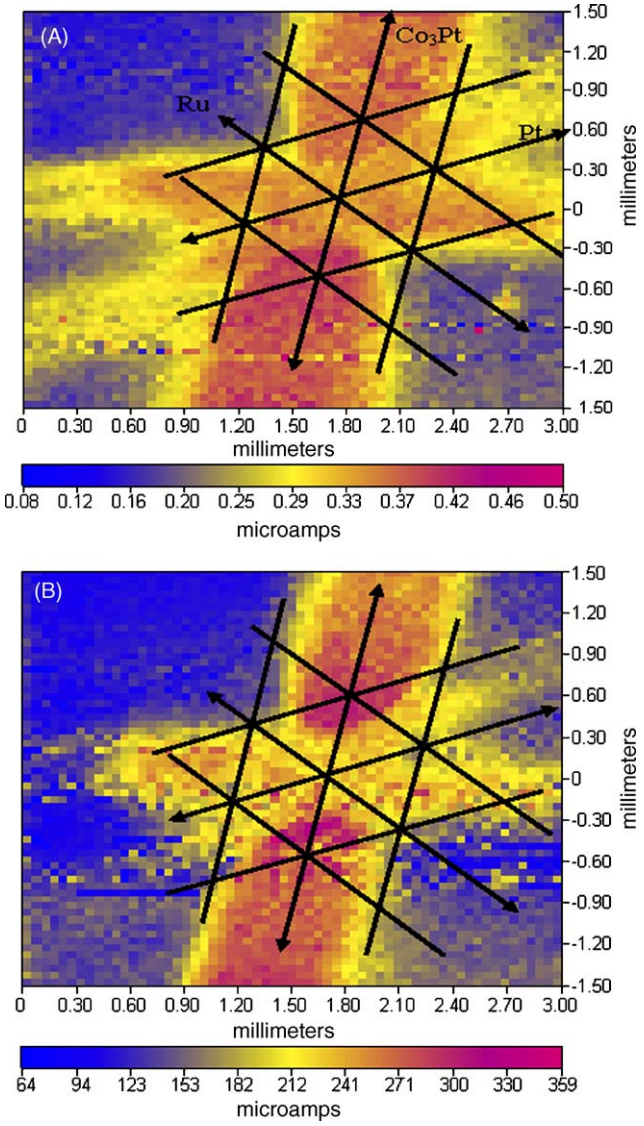

Fig. 9. SECM area scan images for a Pt–Ru–Co_3Pt thin film cross before (A) and after CO poisoning (B). $i_{T,\infty}$ is around 340 nA. $E_{tip} = -1\ V_{SCE}$, $E_{sub} = 0\ V_{SCE}$, separation between tip and substrate is 10 μm.

the oxidation and removal of CO from the surface of Pt through the well-known bi-functional mechanism. It is also speculated that the incorporation of Co with Pt–Ru will decrease the CO coverage by changing the CO-Pt adsorption energy through the mechanism of a ligand effect in a ternary alloy because of the co-presence of Ru and Co when they are in certain Ru:Co ratio [1].

Like WC, the stability of Co is a concern. In the electrolyte solution of 0.01 M H_2SO_4 + 0.1 M Na_2SO_4, Co stripes disappeared (were dissolved) immediately after the immersion in the solution. Like in the case of WC, 2 of the 8 Co layers were replaced by Pt layers to improve the corrosion resistance of the Co stripe but still retain the excellent catalytic activity and CO tolerance seen with incorporation of Co in Pt or Pt–Ru. By partially substituting Pt for Co ($PtCo_3$), the corrosion resistance of Co is substantially improved. No apparent surface change occurred for the Co stripe even after immersion in the solution for a week.

The activity of Co_3Pt towards HOR is higher than that of Pt alone, as shown in Fig. 9A. The addition of Pt to the stripe of Co also improved CO poisoning tolerance of Pt, as indicated by Fig. 9B, where Co_3Pt stripes retains most of their activity after CO poisoning.

4. Conclusions

Scanning electrochemical microscopy was used to rapidly screen thin film composition gradient materials libraries for their electrocatalytic activity towards hydrogen oxidation and CO tolerance. Ternary Pt–Ru–WC and Pt–Ru–Co alloys were investigated as anodic materials for PEM fuel cells.

It was observed that, for most ternary Pt–Ru–WC compositions, the addition of WC to Pt or Pt–Ru catalysts can improve their HOR activity and CO tolerance. SECM screening suggests Pt–Ru–WC and Pt–WC can be potential electrocatalysts for PEM fuel cells. The approximate optimum composition is $Pt_{25\pm10}Ru_{5\pm5}(WC)_{70\pm5}$ for the ternary library, and 65–80 at.% WC for the binary Pt–WC library. In a certain composition regions (compositions of $Pt_{25\pm20}Ru_{15\pm15}Co_{60\pm15}$), the addition of Co to Pt or Pt–Ru catalysts can improve their HOR activity and CO tolerance of Pt. The stability of WC and Co in the acid electrolyte can be enhanced by alloying them with Pt.

Although SECM is a versatile and rapid screening tool for the characterization and combinatorial development of catalyst materials for PEM and direct methanol fuel cell systems, the results from this instrumentation as used in the present work are approximate and only semi-quantitative. The exact optimum composition could not be determined from the SECM data. But rather these data can guide and direct further, more compositionally specific investigations. Processing of "compositionally zoomed" libraries which expand the active regions can be used to better define optimal compositions. Alternatively, synthesis of discrete composition catalyst libraries based on the SECM results can be characterized by multichannel microelectrode systems [29] and real catalyst nanoparticles of the optimum compositions thereafter obtained can be prepared with some other routes and tested in a real fuel cell environment, as the final step for the catalyst development.

Acknowledgements

This work described herein was financially supported by the U.S. Army CECOM RDEC through Agreement No. DAAB07-03-3-K414. Such support does not constitute endorsement by the U.S. Army of the views expressed in this publication. It was also partially supported through funding from the Indiana 21st Century Research and Technology Fund.

The authors are grateful to Nancy Finnegan for all of the work with AES that was carried out in the Center for Microanalysis of Materials, University of Illinois, which is partially supported by the U.S. Department of Energy under grant DEFG02-91-ER45439.

References

[1] P. Strasser, Q. Fan, M. Devenney, W.H. Weinberg, P. Liu, J.K. Norskov, J. Phys. Chem. B. 107 (2003) 11013.
[2] K. Jambunathan, B.C. Shah, J.L. Hudson, A.C. Hillier, J. Electroanal. Chem. 500 (2000) 279.
[3] H.H. Hwu, B.D. Polizzotti, J.G. Chen, J. Phys. Chem. B 105 (2001) 10045.
[4] T. Frelink, W. Visscher, J.A.R. van Veen, J. Electroanal. Chem. 382 (1995) 65.
[5] B. Beden, F. Kadirgan, C. Lamy, J.M. Lager, J. Electroanal. Chem. 127 (1981) 75.
[6] M. Gotz, H. Wendt, Electrochim. Acta 43 (1998) 3637.
[7] K.L. Ley, R. Liu, C. Pu, Q. Fan, N. Leyarovska, C. Segre, E.S. Smotkin, J. Electrochem. Soc. 144 (1997) 1543.
[8] H.H. Hwu, J.G. Chen, K. Kourtakis, J.G. Lavin, J. Phys. Chem. B 105 (2001) 10037.
[9] M.B. Zellner, J.G. Chen, J. Electrochem. Soc. 152 (2005) A1483.
[10] C.J. Barnett, G.T. Burstein, A.R.J. Kucernak, K.R. Williams, Electrochim. Acta 42 (1997) 2381.
[11] D.R. McIntyre, G.T. Burstein, A. Vossen, J. Power Sources 107 (2002) 67.
[12] R. Ganesan, J.S. Lee, Angewandt Chemie Int, Ed. 44 (2005) 6557.
[13] R. Venkataraman, H.R. Kunz, J.M. Fenton, J. Electrochem. Soc. 150 (2003) A278.
[14] X.G. Yang, C.Y. Wang, Appl. Phys. Lett. 86 (2005) 224104.
[15] P. Zoltowski, Electrochim. Acta 31 (1986) 103.
[16] K. Lee, A. Ishihara, S. Mitsushima, N. Kamiya, K.-I. Ota, Electrochim. Acta 49 (2004) 3479.
[17] T. Page, R. Johnson, J. Hormes, S. Noding, B. Rambaru, J. Electroanal. Chem. 485 (2000) 34.
[18] J.R.C. Salgado, E. Antolini, E.R. Gonzalez, Appl. Catal. B: Environ. 57 (2005) 283.
[19] H.A. Gasteiger, S.S. Kocha, B. Sompalli, F.T. Wagner, Appl. Catal. B: Environ. 56 (2005) 9.
[20] X.-D. Xiang, X. Sun, G. Briceno, Y. Lou, K.-A. Wang, H. Chang, W.G. Wallace- Freedman, S.-W. Chen, P.G. Schultz, Science 268 (1995) 1738.
[21] E. Reddington, A. Sapienza, B. Gurau, R. Viswanathan, S. Sarangapani, E.S. Smotkin, T.E. Mallouk, Science 280 (1998) 1735.
[22] R. Jiang, D. Chu, J. Electroanal. Chem. 527 (2002) 137.
[23] J. Zhou, Y. Zu, A.J. Bard, J. Electroanal. Chem. 491 (2000) 22.
[24] S. Jayaraman, A.C. Hillier, J. Com. Chem. 6 (2004) 27.
[25] M. Black, J. Cooper, P. McGinn, Chem. Eng. Sci. 59 (2004) 4839.
[26] M. Black, J. Cooper, P. McGinn, Meas. Sci. Technol. 16 (2005) 174.
[27] J.S. Cooper, G. Zhang, P. McGinn, Rev. Scientific Instruments 76 (2005) 062221.

[28] A.J. Bard, M.V. Mirkin, Scanning Electrochemical Microscopy, Marcel Dekker, New York, 2001.
[29] J.S. Cooper, P. McGinn, Unpublished multichannel microelectrode data for Pt–Ru–WC ternary systems.
[30] H.H. Hwu, J.G. Chen, J. Phys. Chem. B 107 (2003) 2029.
[31] E. Ticianelli, J.B. Beery, M.T. Paffett, S. Gottesfeld, J. Electroanal. Chem. 258 (1989) 61.
[32] T. Kawaguchi, W. Sugimoto, Y. Murakami, Y. Takasu, Electrochem. Comm. 6 (2004) 480.
[33] M.C. Perez, A. Rincon, C. Gutierrez, J. Electroanal. Chem. 511 (2001) 39.
[34] R. Venkataraman, H.R. Kunz, J.M. Fenton, J. Electrochem. Soc. 150 (2003) A278.
[35] P. Zoltowski, Electrochim. Acta 37 (1992) 447.
[36] M.B. Zellner, J.G. Chen, Catal. Today 99 (2005) 299.